

Photoemission and Dynamical Mean Field Theory Study of Electronic Correlation in a t_{2g}^5 Metal of SrRhO₃ Thin Film

Yujun Zhang,^{1,2,*} Minjae Kim,^{3,4,†} Jernej Mravlje,⁵ Changhee Sohn,⁶ Yongseong Choi,⁷ Joerg Stremper,⁷ Yasushi Hotta,⁸ Akira Yasui,⁹ John Nichols,¹⁰ Ho Nyung Lee,⁶ and Hiroki Wadati^{1,2}

¹Graduate School of Materials Science, University of Hyogo,
3-2-1 Kouto, Kamigori-cho, Ako-gun, Hyogo 678-1297, Japan

²Institute for Solid State Physics, University of Tokyo, 5-1-5 Kashiwanoha, Chiba 277-8581, Japan

³Department of Physics and Astronomy, Rutgers University, Piscataway, New Jersey 08854, USA

⁴Collège de France, 11 place Marcelin Berthelot, 75005 Paris, France

⁵Jožef Stefan Institute, Jamova 39, Ljubljana, Slovenia

⁶Materials Science and Technology Division, Oak Ridge National Laboratory, Oak Ridge, Tennessee 37831, USA

⁷Advanced Photon Source, Argonne National Laboratory, Argonne, Illinois 60439, USA

⁸Department of Engineering, University of Hyogo, 2167 Shosha, Himeji, Hyogo 671-2280, Japan

⁹Japan Synchrotron Radiation Research Institute (JASRI), 1-1-1 Kouto, Sayo, Hyogo 679-5198, Japan

¹⁰Department of Physics and Astronomy, University of Arkansas at Little Rock, Little Rock, AR, 72204, USA

Perovskite rhodates are characterized by intermediate strengths of both electronic correlation as well as spin-orbit coupling (SOC) and usually behave as moderately correlated metals. A recent publication (Phys. Rev. B 95, 245121(2017)) on epitaxial SrRhO₃ thin films unexpectedly reported a bad-metallic behavior and suggested the occurrence of antiferromagnetism below 100 K. We studied this SrRhO₃ thin film by hard x-ray photoemission spectroscopy and found a very small density of states (DOS) at Fermi level, which is consistent with the reported bad-metallic behavior. However, this negligible DOS persists up to room temperature, which contradicts with the explanation of antiferromagnetic transition at around 100 K. We also employed electronic structure calculations within the framework of density functional theory and dynamical mean-field theory. In contrast to the experimental results, our calculations indicate metallic behavior of both bulk SrRhO₃ and the SrRhO₃ thin film. The thin film exhibits stronger correlation effects than the bulk, but the correlation effects are not sufficient to drive a transition to an insulating state. The calculated uniform magnetic susceptibility is substantially larger in the thin film than that in the bulk. The role of SOC was also investigated and only a moderate modulation of the electronic structure was observed. Hence SOC is not expected to play an important role for electronic correlation in SrRhO₃.

INTRODUCTION

4d transition metal compounds are characterized by the moderate strengths of both electronic correlation and spin-orbit coupling (SOC) compared to their strongly correlated 3d and strongly spin-orbit-coupled 5d counterparts. Nevertheless, 4d systems do exhibit interesting physical properties as well. Notable examples are found especially in the perovskite ruthenate family: unconventional superconductivity in Sr₂RuO₄ [1, 2], ferromagnetism (FM) in SrRuO₃ [3], and current-induced insulator-metal transition in Ca₂RuO₄ [4, 5], etc. Magnetism plays an important role in many 4d systems. Spin-triplet superconductivity in Sr₂RuO₄ was argued to be related to ferromagnetic spin fluctuations [1, 2]. FM is realized in SrRuO₃ [3] while CaRuO₃ [6] and Sr₃Ru₂O₇ [7, 8] are presumably close to FM. On the other hand, Ca₂RuO₄ is a special case that exhibits an antiferromagnetic (AFM) insulating ground state and insulator-metal transition [9, 10]. However, generally magnetic ordering is rarely observed in other perovskite 4d oxides [11, 12].

Since Rh is the neighbour of Ru in the 4d transition metal series, Rh-based perovskite oxides, such as SrRhO₃ [13–16], Sr₂RhO₄ [17–20] and Sr₃Rh₂O₇ [21],

have also attracted considerable research attention. In the bulk state, these rhodates are usually correlated metals without magnetic ordering. Among them, SrRhO₃ has the most simple crystal structure. As first reported by Yamaura *et al.* [13], bulk SrRhO₃ has a GdFeO₃-type distorted perovskite structure with space group *Pnma*. Metallic transport behavior was observed down to 1.8 K [13] and covalent doping of Ca at the Sr-site does not have significant influence on the metallic state of SrRhO₃ [14]. Nevertheless, there are several reports that strongly indicate the instability towards magnetic ordering in SrRhO₃. An enhanced paramagnetic susceptibility [13] and related theoretical investigations [15] indicate that SrRhO₃ is near a quantum critical point with significant ferromagnetic quantum fluctuation.

Recently, epitaxial SrRhO₃ thin films were successfully synthesized and their transport and magnetic properties were reported by Nichols *et al.* [16]. No FM was observed in the SrRhO₃ thin films but subtle anomalies appeared at around 100 K in magnetization and magnetoresistance, which indicates the possibility of a magnetic transition. Based on density functional theory (DFT) +*U* calculations, Ref. [16] suggested that a C-type AFM structure is energetically favorable. One remarkable result from Ref. [16] is that the resistivity of SrRhO₃ is

very weakly dependent on temperature at high temperature and exhibits an upturn upon cooling below 100 K, showing a weakly insulating behavior. Although this behavior is probably related to some AFM order, there is no direct experimental confirmation about this point so far.

In the present work, we studied SrRhO₃ epitaxial thin film by hard x-ray photoemission spectra (HAXPES) to characterize its electronic structure and the correlation effects, as was earlier done for other perovskite transition metal oxides in Refs. [12, 22–24]. Instead of a coherent peak, a negligible density of states (DOS) near Fermi level (E_F) was observed. This is the case for the results both at room temperature and at 80 K, which precludes the interpretation of the resistivity upturn upon cooling for temperature around 100 K in terms of the gap opening induced by AFM order. Realistic dynamic mean field theory (DMFT) calculations were conducted to investigate the electronic correlation and instability towards magnetic ordering in the SrRhO₃ thin film. Since SOC can also play a significant role to influence the electronic structure of 4d perovskite oxides such as Sr₂RuO₄ [18, 25] and Sr₂RhO₄ [18–20], the possible effects of SOC are investigated and discussed as well.

METHODS

A 9 nm-thick epitaxial SrRhO₃ thin film was grown on a SrTiO₃(001) single crystalline substrate by pulsed laser deposition. The details of the fabrication methods and basic characterization of the sample were previously reported in Ref. [16].

HAXPES of the SrRhO₃ thin film was measured at BL47XU of SPring-8. The incidence angle of linearly polarized (π -polarization) 7.94 keV hard x-ray was set at 1° and photoemission spectra were collected by a Scienta R-4000 electron energy analyzer with an energy resolution of around 250 meV. Surface-sensitive soft x-ray photoemission spectra (SX PES) were measured by a PHI 5000 VersaProbe system (ULVAC-PHI Inc.) with perpendicular incidence of Al $K\alpha$ radiation (1468.7 eV). The energy resolution of the SX PES measurement was around 450 meV. The position of E_F and the energy resolution of both photoemission measurements were determined by measuring and fitting the spectra of a Au reference sample, which was in electrical contact with the SrRhO₃ thin film. For temperature dependent HAXPES measurement, a He-flow cryostat was employed to cool the sample down to 80 K.

X-ray linear dichroism (XLD) and resonant magnetic x-ray diffraction (RMXD) measurements of the SrRhO₃ thin film at the Rh L edge were carried out at beamline 4-ID-D of Advanced Photon Source. For the room temperature XLD measurement, linearly polarized x-rays with electric field component E perpendicular and par-

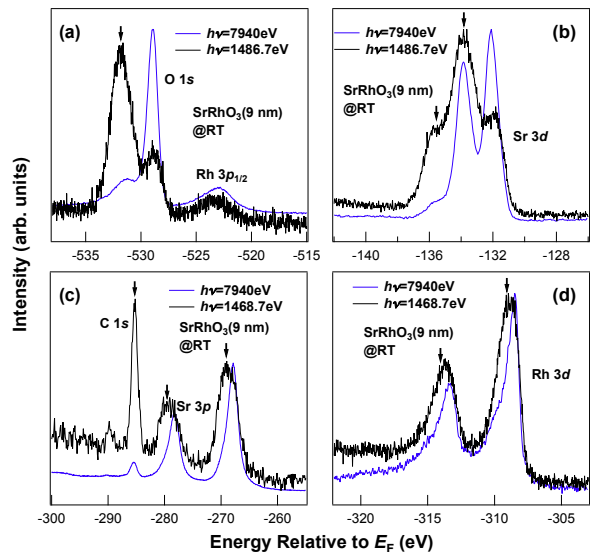


FIG. 1. Room temperature (a) O 1s and Rh 3p_{1/2}; (b) Sr 3d; (c) C 1s and Sr 3p; (d) Rh 3d core level photoemission spectra of the SrRhO₃ thin film. The arrows indicate the surface components, which are enhanced in SX PES.

allel to the sample surface were utilized to measure the x-ray absorption spectra (XAS). The incidence angle of the x-rays was set at around 3° and the XAS signal was collected by partial fluorescence yield mode. RXMD measurement was conducted at 30 K by cooling the sample with an ARS He Displex cryocooler.

For the DFT calculation, we used the Wien2k package [26] and local density approximation (LDA) was employed for the calculation of the exchange correlation potential. For the DFT+DMFT calculation, we used the TRIQS framework [27–30] and treated t_{2g} orbitals by using a rotationally invariant Kanamori Hamiltonian with parameters $U = 2.3$ eV and $J = 0.4$ eV, which has been used to precisely describe the neighbouring ruthenates [31, 32]. To compute the magnetic susceptibility by DFT+DMFT, we applied a magnetic field of 5 meV (around 86 T) and allowed symmetry breaking of spin up and down. For crystal structure optimization of the SrRhO₃ thin film, we assumed the in-plane symmetry and lattice constants of the SrTiO₃ substrate and relaxed the internal positions of atoms in the unit cell by using DFT [16].

PHOTOEMISSION RESULTS

Fig. 1 shows the core level HAXPES and SX PES results of the SrRhO₃ thin film. HAXPES is quite bulk-sensitive and the detection depth is beyond the thickness of the film since the photoemission signal of Ti in the substrate can be observed. On the other hand, SX PES is very surface sensitive, whose typical detection depth is around

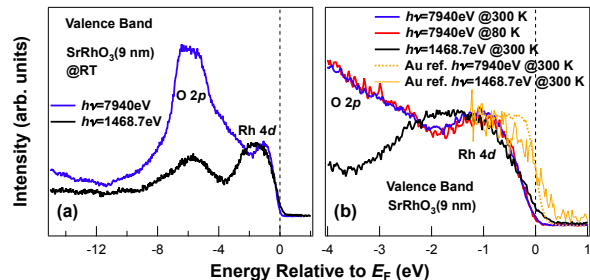


FIG. 2. (a) Room temperature valence band photoemission spectra of the SrRhO₃ thin film. (b) Enlarged valence band photoemission spectra of the SrRhO₃ thin film. The data of reference Au are also shown.

1 to 2 nm [33]. It can be noticed in Fig.1 that surface components (-532 eV O 1s peak in Fig.1(a); -135.7 eV/-133.9 eV Sr 3d peaks in Fig.1(b); C 1s contamination signal at -285.5 eV in Fig.1(c); left shoulders of Sr 3p in Fig.1(c) and left shoulders of Rh 3d in Fig.1(d)) have different binding energies compared to the bulk components (-528.9 eV O 1s peak in Fig.1(a); -133.9 eV/-132.1 eV Sr 3d peaks in Fig.1(b); main peaks of Sr 3p at -278.2 eV/-267.9 eV in Fig.1(c) and main peaks of Rh 3d at -313.3 eV/-308.5 eV in Fig.1(d)). The surface components have little influence on the HAXPES results. The binding energies of peaks in the Rh 3d spectra are also consistent with previous reports of Rh⁴⁺ oxides [34].

The valence band HAXPES and SXPES results are displayed in Fig.2(a). Due to the different photoionization cross section of *p* and *d* levels for hard and soft x-rays [35], HAXPES is more sensitive to *p* levels and SXPES is more sensitive to *d* levels. By comparing the HAXPES and SXPES results, it can be concluded that the features in the energy range from -10 eV to -3 eV are dominated by O 2*p* emission and the features above -3 eV mainly come from Rh 4*d* emission. Fig.2(b) shows the valence band spectra in an expanded region near E_F . Surprisingly, the coherent peak is totally absent for both HAXPES and SXPES. The difference between HAXPES and SXPES at E_F is mainly due to the different energy resolution of HAXPES and SXPES. By comparing with the corresponding spectra of the Au reference sample, it is clear that both HAXPES and SXPES have negligible intensity at E_F . It should be noted that the SrTiO₃ substrate could also contribute to the HAXPES valence band spectra due to the large detection depth of HAXPES. However, since SrTiO₃ is an insulator with *d*⁰ configuration, it has nearly no contribution to the intensity above -3 eV [36].

In Ref. [16], the possibility of magnetic ordering in the SrRhO₃ thin film with a transition temperature of around 100 K was proposed. To investigate the temperature dependence of the electronic structure in the SrRhO₃ thin film, we also conducted HAXPES measurement at

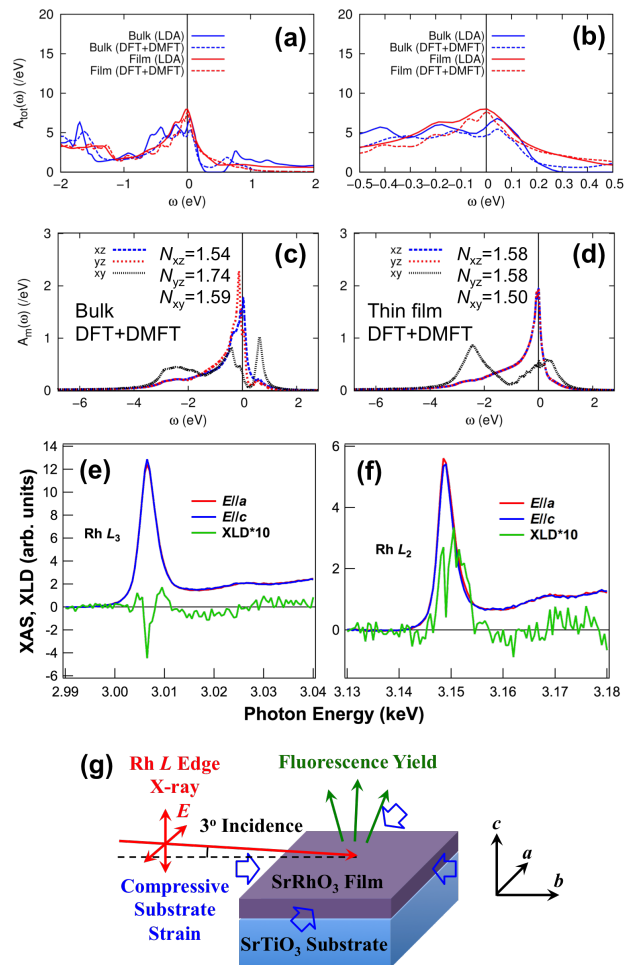


FIG. 3. Total DOS $A_{tot}(\omega)$ calculated by DFT and DFT+DMFT ($T=58$ K) for the bulk and the thin film in (a) wider energy range and (b) narrower energy range. Orbital resolved DFT+DMFT DOS $A_m(\omega)$ at $T=58$ K for (c) the bulk and (d) the thin film. N in the figures indicates the orbital occupation. ω is the energy relative to E_F . (e,f) Rh *L* edge XAS and XLD spectra of the SrRhO₃ thin film. (g) Schematic of the XLD measurement for the SrRhO₃ thin film under compressive substrate strain.

80 K. However, nearly no temperature dependence was observed, as shown in Fig.2(b). Since the SrTiO₃ substrate has a structural phase transition near this temperature [37], the reported anomalies in transport properties [16] may be related to the change of substrate strain rather than a real magnetic transition. Consequently, the valence band structure of the SrRhO₃ thin film does not show a significant temperature dependence.

DFT AND DFT+DMFT RESULTS

The photoemission results above suggest negligibly small DOS near E_F in the SrRhO₃ thin film, in contrast to bulk SrRhO₃ that exhibits metallic behavior [13]. In

order to understand this phenomenon, we now turn to the DFT(+DMFT) calculations, performed for both the bulk and the thin film.

The total DOS obtained by DFT+DMFT is shown in Fig.3(a,b). One can notice that DFT+DMFT calculations predict metallic behavior for both the bulk and the thin film. Only moderate effects of electronic correlation with renormalization of $Z \approx 0.5$ are observed ($Z = (1 - \frac{\partial \text{Re}\Sigma(\omega)}{\partial \omega})^{-1}|_{\omega \rightarrow 0}$), as obtained by the self-energy results shown in Fig.4. The thin film is slightly more correlated with smaller values of Z , but no major difference between the thin film and the bulk is observed, in contrast to the experimental results.

According to the orbitally resolved DFT+DMFT DOS in Fig.3(c,d), due to the larger bandwidth of the xy orbital than that of the xz/yz orbitals, the occupancy of the xy orbital (1.50) is smaller than that of the xz/yz orbitals (1.58) in the thin film, which is consistent with the Rh L_2 edge XLD results. As depicted in Fig.3(e-g), XLD is defined as the difference of XAS measured by using incident x-rays with $E//a$ and $E//c$, where a and c are the in-plane [100] and the out-of-plane [001] directions, respectively. Since the XAS intensity at the Rh L edge is proportional to the number of $4d$ holes, a positive XLD signal indicates a preferred occupation of out-of-plane $4d$ orbitals and less occupation of in-plane $4d$ orbitals. Note that the sign change in the L_3 edge XLD spectrum could often be observed in other systems as well, while the spectrum at the L_2 edge can usually reflect the orbital occupation more unambiguously [38]. These experimental and calculation results are consistent with the biaxial compressive strain from the SrTiO₃ substrate [16].

On the other hand, in contrast to the strong orbital anisotropy of spectral weight in between the xy and the xz/yz orbitals, the orbital dependence of quasi-particle renormalization is not as strong as that in Sr₂RuO₄ [31, 39], which is consistent with the claim in Ref. [40] that correlation effects are weaker in SrRhO₃ than in perovskite ruthenates. The electronic correlation changes the effective energy level of the xz , yz , and xy orbitals. In the DFT calculation, the center energy of the xy orbital is 618 meV higher than that of the xz/yz orbitals in the SrRhO₃ thin film. In the DFT+DMFT self-energy of the thin film (Fig.4(b)), the xz/yz orbitals are shifted up with respect to the xy level for 212 meV, as shown by the difference of the real part of self-energy at zero energy. As a result, the effective energy level of xy with respect to that of xz/yz is reduced from 618 meV to 404 meV by electronic correlation in DFT+DMFT calculations. Since the Van-hove peaks of the xz/yz orbitals in DFT are close to E_F within 30 meV (Fig.3(a,b)), the correlation-induced shift-up of the xz/yz orbitals gives rise to the reduction of the DOS at E_F in DFT+DMFT, as shown in Fig.5(a). Both the bulk and the thin film show a similar trend that the total DOS at E_F is reduced

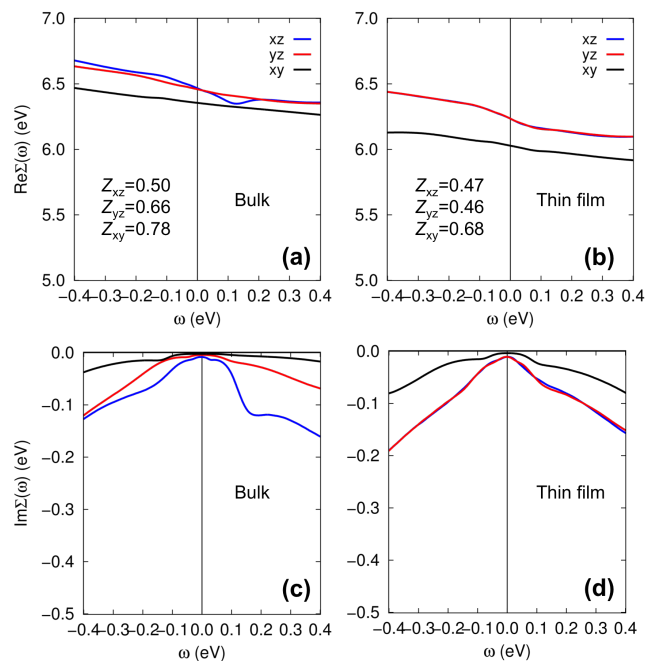


FIG. 4. DFT+DMFT self-energy for the bulk and the thin film at $T=58$ K. (a) Real part, bulk; (b) Real part, thin film; (c) Imaginary part, bulk; (d) Imaginary part, thin film. Corresponding renormalization factors Z are listed in the figures.

by correlation, which is qualitatively consistent with the small electronic component of the experimental specific heat of SrRhO₃ [13]. It is noteworthy that the xz/yz orbitals have a larger DOS at E_F than the xy orbital in the thin film. Meanwhile, the result that $Z \approx 0.5$ for all orbitals implies that electronic correlation is not so sensitive to the value of the DOS at small energies, which is different from Hund's metals such as ruthenates and iron-based superconductors [31, 41].

We also calculated the uniform magnetic susceptibility of both the bulk and the thin film, as shown in Fig.5(b). In contrast to the self-energy, the calculated magnetic susceptibility does show a substantially different behavior in the thin film. The magnetic susceptibility of the thin film is 6 to 7 times larger and exhibits a stronger temperature dependence than that of the bulk case, in contrast to the nearly temperature independent total DOS in the bulk and the thin film (Fig.5(a)). The difference in the calculated magnetic susceptibility for the bulk and the thin film can be understood as follows. First, the larger total DOS at E_F in the thin film with respect to that in the bulk (Fig.3(b)) gives rise to a larger magnetic susceptibility. Second, the stronger electronic correlation of the xz/yz orbitals in the thin film compared to that in the bulk (Fig.4(a-d)) gives rise to a larger magnetic instability in the thin film. Third, the sharper slope in the DOS of the xz/yz orbitals in the thin film compared to

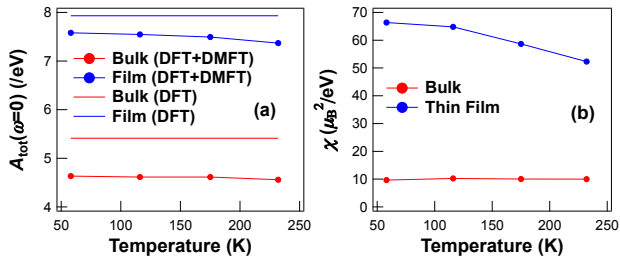


FIG. 5. (a) Temperature dependent total DFT+DMFT DOS at E_F for the bulk and the thin film. The total DOS calculated by DFT for the bulk and the thin film are also plotted for comparison. (b) Temperature dependent magnetic susceptibility calculated by DFT+DMFT for the bulk and the thin film.

that in the bulk (Fig.3(c,d)) gives rise to a stronger temperature dependence of the magnetic susceptibility in the thin film. These results are inherited from the tetragonal symmetry of the lattice of the thin film, which gives rise to the presence of the Van-hove singularity of the xz/yz orbitals near Fermi level.

In our photoemission results, it is clearly shown that there is a negligible temperature dependence of the DOS between 80 K and 300 K. The present DFT+DMFT results with similar renormalization for both the bulk and thin film suggest that if there is a real transition of the electronic structure, it will not be a simple metal-insulator transition with a Mott gap. The larger magnetic susceptibility in the thin film compared to that in the bulk implies that the SrRhO_3 thin film has a much stronger intrinsic instability towards magnetically ordered phases. This magnetic instability is mainly induced by the anisotropy of the crystal environment, such as crystal field symmetry and bandwidth anisotropy. However, whether this larger magnetic susceptibility is a side effect (or indicator) of some actual electronic instability that in turn is responsible for the experimentally observed negligible DOS at E_F is an open question.

Earlier DFT calculations reported the occurrence of an AFM state in SrRhO_3 thin films [16]. We investigated the possibility of magnetic ordering by DFT+ U calculation and found that we need $U > 5$ eV for the stabilization of the C-type AFM state, which is too large for the $4d$ shell [42, 43]. We also conducted RXMD experiments at the Rh L edges to attest the existence of AFM ordering peaks. Due to the restricted Q range that the Rh L edge x-ray (around 3 keV) can reach, Q vectors of (0 0 0.5) (A-type), (0.5 0.5 1) (C-type) and (0.5 0.5 0.5) (G-type) were investigated at 30 K but no observable diffraction appeared within the detection limit.

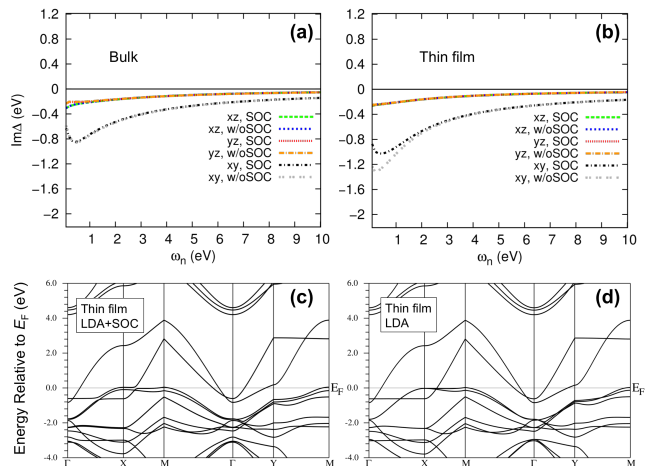


FIG. 6. Hybridization functions in the initial step of DFT+DMFT calculation for (a) the bulk and (b) the thin film. ω_n is the Matsubara frequency. Band structures for the thin film calculated by DFT (c) with and (d) without SOC.

ABOUT NEGLIGIBLE DOS AT E_F IN SrRhO_3 THIN FILM: SOC, ORDERING AND BEYOND

In principle, a possible origin of the small value of measured DOS at E_F and the absence of a coherent peak could be SOC, which can play an important role in t_{2g}^5 iridates [44, 45]. If SOC were strong enough to split the $J_{\text{eff}} = 1/2$ and $J_{\text{eff}} = 3/2$ states significantly, one could expect that an insulating behavior would be promoted by the half-filled $J_{\text{eff}} = 1/2$ band. We are unable to run the DFT+DMFT calculation in the presence of SOC because of the fermionic sign problem in the quantum impurity solver [29, 30]. But to get a first impression of the possible role of SOC, we calculated the hybridization functions, which determine the behavior of the DMFT calculation in the presence of SOC. The results shown in Fig.6(a,b) imply that SOC moderately affects the electronic structure of SrRhO_3 . As also shown by DFT results with and without SOC in Fig.6(c,d), in the thin film, due to the SOC-induced band splitting around E_F (along Γ to X line), SOC reduces the hybridization function of the xy orbital for a small energy scale of 1 to 2 eV (Fig.6(b)). Provided the fact that quasiparticle residue $Z \approx 0.5$ and a small orbital dependence of the Fermi velocity, we suggest that SOC can not trigger the metal-insulator transition but might give rise to a strong magnetic instability in the SrRhO_3 thin film. For bulk SrRhO_3 , the effect of SOC is even smaller due to the lower lattice symmetry, as shown in Fig.6(a). Note that even in SrIrO_3 , the $5d$ counterpart of SrRhO_3 , SOC is still not strong enough to trigger an insulating behavior [45]. Moreover, we can get similar conclusion by analyzing the branching ratio (BR) of XAS results shown in Fig.3(e,f). The BR between the white-line intensities of

Rh L_3 and L_2 edges is related to the ground-state expectation value of the angular part of SOC [46]. A large deviation from the statistical BR=2 indicates the presence of strong SOC effects. The experimental BR at the Rh $L_{3,2}$ edges is close to the statistical value of 2 (estimated as around 2.3 from Fig.3(e,f)), indicating weak SOC effects in the SrRhO₃ thin film. This is in contrast to the Ir $5d$ cases where large deviations (BR > 4) from the statistical value, thus large SOC, have been observed [47–49].

There is also the possibility of more complicated magnetic or charge ordering, such as helical magnetic ordering or spin/charge density waves, which could be responsible for the absence of coherent peak in the SrRhO₃ thin film. Another possible mechanism could be formation of polarons induced by electron-phonon interaction. These possibilities should be considered and investigated in future to further clarify the electronic structure of SrRhO₃ thin films.

CONCLUSIONS

In summary, we experimentally and theoretically investigated the effects of electronic correlation in SrRhO₃. The photoemission results indicate a negligible DOS at E_F in the SrRhO₃ thin film with little temperature dependence. We considered SrRhO₃ within band-structure calculation taking into account the electronic correlation with a DFT+DMFT approach. In our calculation the small DOS at E_F could not be reproduced, rather a moderately correlated metallic behavior was observed. Our attempts to detect the AFM magnetic diffraction by experiment and to stabilize magnetically ordered states in the calculations both failed. But the calculation did reveal an interesting behavior in the magnetic susceptibility that is substantially larger for the thin film. This result is mainly induced by the difference of crystal anisotropy between the bulk and the thin film. Further investigations are welcome to identify the possible magnetic ordering and clarify the effects of SOC in SrRhO₃. Moreover, $5d$ transition metal oxides, such as SrIrO₃ or Sr₂IrO₄, have strong SOC effects on the electronic correlation [50]. We are also looking forward to comparative theoretical studies on them.

ACKNOWLEDGEMENTS

This work was supported by Grant-in-Aid for JSPS fellows (No. 17F17327). The HAXPES experiments at SPring-8 were performed under the approval of the Japan Synchrotron Radiation Research Institute (Proposal No. 2018B1449). This research used resources of the Advanced Photon Source, a U.S. Department of Energy (DOE) Office of Science User Facility operated for the DOE Office of Science by Argonne National Labo-

ratory under Contract No. DE-AC02-06CH11357. The work at ORNL was supported by the U.S. Department of Energy, Office of Science, Basic Energy Sciences, Materials Sciences and Engineering Division. M. K. acknowledges support from Grant No. NSF DMR-1733071, and grateful to CPHT computer support team. We are thankful to the support and advices provided by A. Georges, V. R. Cooper, S. F. Yuk, and A. Rastogi. And we also acknowledge the support provided by K. Ikeda, S. Sakuragi and H. Kinoshita, as well as enlightening discussion about this work with J. W. Kim and H. Zhou during our beamtime in Advanced Photon Source.

* zhangyujun@issp.u-tokyo.ac.jp

† garix.minjae.kim@gmail.com

- [1] Y. Maeno, H. Hashimoto, K. Yoshida, S. Nishizaki, T. Fujita, J. G. Bednorz, and F. Lichtenberg. Superconductivity in a layered perovskite without copper. *Nature*, 372(6506):532, 1994.
- [2] A. P. Mackenzie and Y. Maeno. The superconductivity of Sr₂RuO₄ and the physics of spin-triplet pairing. *Reviews of Modern Physics*, 75(2):657, 2003.
- [3] A. Kanbayasi. Magnetic properties of SrRuO₃ single crystal. *Journal of the Physical Society of Japan*, 41(6):1876–1878, 1976.
- [4] F. Nakamura, M. Sakaki, Y. Yamanaka, S. Tamaru, T. Suzuki, and Y. Maeno. Electric-field-induced metal maintained by current of the Mott insulator Ca₂RuO₄. *Scientific Reports*, 3:2536, 2013.
- [5] C. Sow, S. Yonezawa, S. Kitamura, T. Oka, K. Kuroki, F. Nakamura, and Y. Maeno. Current-induced strong diamagnetism in the Mott insulator Ca₂RuO₄. *Science*, 358(6366):1084–1087, 2017.
- [6] G. Cao, S. McCall, M. Shepard, J. E. Crow, and R. P. Guertin. Thermal, magnetic, and transport properties of single-crystal Sr_{1-x}Ca_xRuO₃ (0 ≤ x ≤ 1.0). *Physical Review B*, 56(1):321, 1997.
- [7] G. Cao, S. McCall, and J. E. Crow. Observation of itinerant ferromagnetism in layered Sr₃Ru₂O₇ single crystals. *Physical Review B*, 55(2):R672, 1997.
- [8] S. Ikeda, Y. Maeno, S. Nakatsuji, M. Kosaka, and Y. Uwatoko. Ground state in Sr₃Ru₂O₇: Fermi liquid close to a ferromagnetic instability. *Physical Review B*, 62(10):R6089, 2000.
- [9] S. Nakatsuji, S. Ikeda, and Y. Maeno. Ca₂RuO₄: New Mott insulators of layered ruthenate. *Journal of the Physical Society of Japan*, 66(7):1868–1871, 1997.
- [10] J. P. Carlo, T. Goko, I. M. Gat-Malureanu, P. L. Russo, A. T. Savici, A. A. Aczel, G. J. MacDougall, J. A. Rodriguez, T. J. Williams, G. M. Luke, C. R. Wiebe, Y. Yoshida, S. Nakatsuji, Y. Maeno, T. Taniguchi, and Y. J. Uemura. New magnetic phase diagram of (Sr,Ca)₂RuO₄. *Nature Materials*, 11(4):323, 2012.
- [11] D. Oka, Y. Hirose, S. Nakao, T. Fukumura, and T. Hasegawa. Intrinsic high electrical conductivity of stoichiometric SrNbO₃ epitaxial thin films. *Physical Review B*, 92(20):205102, 2015.

- [12] H. Wadati, J. Mravlje, K. Yoshimatsu, H. Kumigashira, M. Oshima, T. Sugiyama, E. Ikenaga, A. Fujimori, A. Georges, A. Radetinac, K. S. Takahashi, M. Kawasaki, and Y. Tokura. Photoemission and DMFT study of electronic correlations in SrMoO₃: Effects of Hund's rule coupling and possible plasmonic sideband. *Physical Review B*, 90(20):205131, 2014.
- [13] K. Yamaura and E. Takayama-Muromachi. Enhanced paramagnetism of the 4d itinerant electrons in the rhodium oxide perovskite SrRhO₃. *Physical Review B*, 64(22):224424, 2001.
- [14] D. J. Singh. Prospects for quantum criticality in perovskite SrRhO₃. *Physical Review B*, 67(5):054507, 2003.
- [15] K. Yamaura, Q. Huang, D. P. Young, M. Arai, and E. Takayama-Muromachi. Electronic properties of the novel 4d metallic oxide SrRhO₃. *Physica B: Condensed Matter*, 329:820–821, 2003.
- [16] J. Nichols, S. F. Yuk, C. Sohn, H. Jeon, J. W. Freeland, V. R. Cooper, and H. N. Lee. Electronic and magnetic properties of epitaxial SrRhO₃ films. *Physical Review B*, 95(24):245121, 2017.
- [17] R. S. Perry, F. Baumberger, L. Balicas, N. Kikugawa, N. J. C. Ingle, A. Rost, J. F. Mercure, Y. Maeno, Z. X. Shen, and A. P. Mackenzie. Sr₂RhO₄: a new, clean correlated electron metal. *New Journal of Physics*, 8(9):175, 2006.
- [18] M. W. Haverkort, I. S. Elfimov, L. H. Tjeng, G. A. Sawatzky, and A. Damascelli. Strong spin-orbit coupling effects on the Fermi surface of Sr₂RuO₄ and Sr₂RhO₄. *Physical Review Letters*, 101(2):026406, 2008.
- [19] G. Q. Liu, V. N. Antonov, O. Jepsen, and O. K. Andersen. Coulomb-enhanced spin-orbit splitting: The missing piece in the Sr₂RhO₄ puzzle. *Physical Review Letters*, 101(2):026408, 2008.
- [20] C. Martins, M. Aichhorn, L. Vaugier, and S. Biermann. Reduced effective spin-orbital degeneracy and spin-orbital ordering in paramagnetic transition-metal oxides: Sr₂IrO₄ versus Sr₂RhO₄. *Physical Review Letters*, 107(26):266404, 2011.
- [21] K. Yamaura, Q. Huang, D. P. Young, Y. Noguchi, and E. Takayama-Muromachi. Crystal structure and electronic and magnetic properties of the bilayered rhodium oxide Sr₃Rh₂O₇. *Physical Review B*, 66(13):134431, 2002.
- [22] M. Takizawa, D. Toyota, H. Wadati, A. Chikamatsu, H. Kumigashira, A. Fujimori, M. Oshima, Z. Fang, M. Lippmaa, M. Kawasaki, and H. Koinuma. Manifestation of correlation effects in the photoemission spectra of Ca_{1-x}Sr_xRuO₃. *Physical Review B*, 72(6):060404, 2005.
- [23] A. Sekiyama, H. Fujiwara, S. Imada, S. Suga, H. Eisaki, S. I. Uchida, K. Takegahara, H. Harima, Y. Saitoh, I. A. Nekrasov, G. Keller, D. E. Kondakov, A. V. Kozhevnikov, T. Pruschke, K. Held, D. Vollhardt, and V. I. Anisimov. Mutual experimental and theoretical validation of bulk photoemission spectra of Sr_{1-x}Ca_xVO₃. *Physical Review Letters*, 93(15):156402, 2004.
- [24] M. Takizawa, M. Minohara, H. Kumigashira, D. Toyota, M. Oshima, H. Wadati, T. Yoshida, A. Fujimori, M. Lippmaa, M. Kawasaki, H. Koinuma, G. Sordi, and M. Rozenberg. Coherent and incoherent *d* band dispersions in SrVO₃. *Physical Review B*, 80(23):235104, 2009.
- [25] M. Kim, J. Mravlje, M. Ferrero, O. Parcollet, and A. Georges. Spin-orbit coupling and electronic correlations in Sr₂RuO₄. *Physical Review Letters*, 120(12):126401, 2018.
- [26] P. Blaha, K. Schwarz, G. K. H. Madsen, D. Kvasnicka, and J. Luitz. An augmented plane wave+ local orbitals program for calculating crystal properties. *Universität Wien, Austria*, 2001.
- [27] M. Aichhorn, L. Pourovskii, P. Seth, V. Vildosola, M. Zingl, O. E. Peil, X. Deng, J. Mravlje, G. J. Kraberger, C. Martins, M. Ferrero, and O. Parcollet. TRIQS/DFTTools: a TRIQS application for *ab initio* calculations of correlated materials. *Computer Physics Communications*, 204:200–208, 2016.
- [28] O. Parcollet, M. Ferrero, T. Ayril, H. Hafermann, I. Krivenko, L. Messio, and P. Seth. TRIQS: A toolbox for research on interacting quantum systems. *Computer Physics Communications*, 196:398–415, 2015.
- [29] P. Seth, I. Krivenko, M. Ferrero, and O. Parcollet. TRIQS/CTHYB: A continuous-time quantum Monte Carlo hybridisation expansion solver for quantum impurity problems. *Computer Physics Communications*, 200:274–284, 2016.
- [30] E. Gull, A. J. Millis, A. I. Lichtenstein, A. N. Rubtsov, M. Troyer, and P. Werner. Continuous-time Monte Carlo methods for quantum impurity models. *Reviews of Modern Physics*, 83(2):349, 2011.
- [31] J. Mravlje, M. Aichhorn, T. Miyake, K. Haule, G. Kotliar, and A. Georges. Coherence-incoherence crossover and the mass-renormalization puzzles in Sr₂RuO₄. *Physical Review Letters*, 106(9):096401, 2011.
- [32] H. T. Dang, J. Mravlje, A. Georges, and A. J. Millis. Electronic correlations, magnetism, and Hund's rule coupling in the ruthenium perovskites SrRuO₃ and CaRuO₃. *Physical Review B*, 91(19):195149, 2015.
- [33] M. P. Seah and W. A. Dench. Quantitative electron spectroscopy of surfaces: A standard data base for electron inelastic mean free paths in solids. *Surface and Interface Analysis*, 1(1):2–11, 1979.
- [34] T. K. Le, D. Flahaut, H. Martinez, N. Andreu, D. Gonbeau, E. Pachoud, D. Pelloquin, and A. Maignan. The electronic structure of the CuRh_{1-x}Mg_xO₂ thermoelectric materials: An x-ray photoelectron spectroscopy study. *Journal of Solid State Chemistry*, 184(9):2387–2392, 2011.
- [35] M. B. Trzhaskovskaya, V. I. Nefedov and V. G. Yarzhevsky. Photoelectron angular distribution parameters for elements Z=1 to Z=54 in the photoelectron energy range 100–5000 eV. *Atomic Data and Nuclear Data Tables*, 77(1):97–159, 2001.
- [36] Y. Haruyama, S. Kodaira, Y. Aiura, H. Bando, Y. Nishihara, T. Maruyama, Y. Sakisaka, and H. Kato. Angle-resolved photoemission study of SrTiO₃ (100) and (110) surfaces. *Physical Review B*, 53(12):8032, 1996.
- [37] N. Ohama, H. Sakashita, and A. Okazaki. The temperature dependence of the lattice constant of SrTiO₃ around the 105 K transition. *Phase Transitions: A Multinational Journal*, 4(2):81–90, 1984.
- [38] D. Pesquera, G. Herranz, A. Barla, E. Pellegrin, F. Bondino, E. Magnano, F. Sanchez, and J. Fontcuberta. Surface symmetry-breaking and strain effects on orbital occupancy in transition metal perovskite epitaxial films. *Nature Communications*, 3:1189, 2012.
- [39] A. Tamai, M. Zingl, E. Rozbicki, E. Cappelli, S. Ricco, A. de la Torre, S. McKeown Walker, F. Y. Bruno, P. D. C. King, W. Meevasana, M. Shi, M. Radovic,

- N. C. Plumb, A. S. Gibbs, A. P. Mackenzie, C. Berthod, H. Strand, M. Kim, A. Georges, and F. Baumberger. High-resolution photoemission on Sr_2RuO_4 reveals correlation-enhanced effective spin-orbit coupling and dominantly local self-energies. ,arXiv:1812.06531, 2018.
- [40] K. Yamaura, D. P. Young, and E. Takayama-Muromachi. Ferromagnetic transition in the correlated $4d$ perovskites $\text{SrRu}_{1-x}\text{Rh}_x\text{O}_3$. *Physical Review B*, 69(2):024410, 2004.
- [41] A. Georges, L. de' Medici, and J. Mravlje. Strong correlations from Hunds coupling. *Annual Review of Condensed Matter Physics*, 4(1):137–178, 2013.
- [42] X. Deng, K. Haule, and G. Kotliar. Transport properties of metallic ruthenates: A DFT+ DMFT investigation. *Physical Review Letters*, 116(25):256401, 2016.
- [43] Z. Fang, N. Nagaosa, and K. Terakura. Orbital-dependent phase control in $\text{Ca}_{2-x}\text{Sr}_x\text{RuO}_4$ ($0 \leq x \leq 0.5$). *Physical Review B*, 69(4):045116, 2004.
- [44] B. J. Kim, H. Jin, S. J. Moon, J.Y. Kim, B.G. Park, C. S. Leem, J. Yu, T. W. Noh, C. Kim, S.J. Oh, J.H. Park, V. Durairaj, G. Cao, and E. Rotenberg. Novel $J_{\text{eff}}=1/2$ Mott state induced by relativistic spin-orbit coupling in Sr_2IrO_4 . *Physical Review Letters*, 101(7):076402, 2008.
- [45] S. J. Moon, H. Jin, K. W. Kim, W. S. Choi, Y. S. Lee, J. Yu, G. Cao, A. Sumi, H. Funakubo, C. Bernhard, and T. W. Noh. Dimensionality-controlled insulator-metal transition and correlated metallic state in $5d$ transition metal oxides $\text{Sr}_{n+1}\text{Ir}_n\text{O}_{3n+1}$ ($n=1, 2$, and ∞). *Physical Review Letters*, 101(22):226402, 2008.
- [46] G. Van der Laan and B. T. Thole. Local probe for spin-orbit interaction. *Physical Review Letters*, 60(19):1977, 1988.
- [47] M. A. Laguna-Marco, D. Haskel, N. Souza-Neto, J. C. Lang, V. V. Krishnamurthy, S. Chikara, G. Cao, and M. van Veenendaal. Orbital magnetism and spin-orbit effects in the electronic structure of BaIrO_3 . *Physical Review Letters*, 105(21):216407, 2010.
- [48] J. P. Clancy, N. Chen, C. Y. Kim, W. F. Chen, K. W. Plumb, B. C. Jeon, T. W. Noh, and Y. J. Kim. Spin-orbit coupling in iridium-based $5d$ compounds probed by x-ray absorption spectroscopy. *Physical Review B*, 86(19):195131, 2012.
- [49] J. W. Kim, Y. Choi, S. H. Chun, D. Haskel, D. Yi, R. Ramesh, J. Liu, and P. J. Ryan. Controlling entangled spin-orbit coupling of $5d$ states with interfacial heterostructure engineering. *Physical Review B*, 97(9):094426, 2018.
- [50] H. Zhang, K. Haule, and D. Vanderbilt. Effective $J=1/2$ insulating state in Ruddlesden-Popper iridates: an LDA+DMFT study. *Physical Review Letters*, 111(24):246402, 2013.